

Article

Spatiotemporal Variability in Wind Turbine Blade Leading Edge Erosion

Sara C. Pryor ^{1,*} , Jacob J. Coburn ¹  and Rebecca J. Barthelmie ² ¹ Department of Earth and Atmospheric Sciences, Cornell University, Ithaca, NY 14853, USA; jjc457@cornell.edu² Sibley School of Mechanical and Aerospace Engineering, Cornell University, Ithaca, NY 14853, USA; rb737@cornell.edu

* Correspondence: sp2279@cornell.edu; Tel.: +1-607-255-3376

Abstract: Wind turbine blade leading edge erosion (LEE) reduces energy production and increases wind energy operation and maintenance costs. Degradation of the blade coating and ultimately damage to the underlying blade structure are caused by collisions of falling hydrometeors with rotating blades. The selection of optimal methods to mitigate/reduce LEE are critically dependent on the rates of coating fatigue accumulation at a given location and the time variance in the accumulation of material stresses. However, no such assessment currently exists for the United States of America (USA). To address this research gap, blade coating lifetimes at 883 sites across the USA are generated based on high-frequency (5-min) estimates of material fatigue derived using a mechanistic model and robust meteorological measurements. Results indicate blade coating failure at some sites in as few as 4 years, and that the frequency and intensity of material stresses are both highly episodic and spatially varying. Time series analyses indicate that up to one-third of blade coating lifetime is exhausted in just 360 5-min periods in the Southern Great Plains (SGP). Conversely, sites in the Pacific Northwest (PNW) exhibit the same level of coating lifetime depletion in over three times as many time periods. Thus, it may be more cost-effective to use wind turbine deregulation (erosion-safe mode) for damage reduction and blade lifetime extension in the SGP, while the application of blade leading edge protective measures may be more appropriate in the PNW. Annual total precipitation and mean wind speed are shown to be poor predictors of blade coating lifetime, re-emphasizing the need for detailed modeling studies such as that presented herein.



Academic Editor: Davide Astolfi

Received: 20 December 2024

Revised: 12 January 2025

Accepted: 14 January 2025

Published: 19 January 2025

Citation: Pryor, S.C.; Coburn, J.J.; Barthelmie, R.J. Spatiotemporal Variability in Wind Turbine Blade Leading Edge Erosion. *Energies* **2025**, *18*, 425. <https://doi.org/10.3390/en18020425>

Copyright: © 2025 by the authors. Licensee MDPI, Basel, Switzerland. This article is an open access article distributed under the terms and conditions of the Creative Commons Attribution (CC BY) license (<https://creativecommons.org/licenses/by/4.0/>).

Keywords: blades; CONUS; hydroclimate; LCoE; LEE; operations and maintenance; Springer model; USA; wind energy

1. Introduction

1.1. Motivation: Wind Turbine Blade Leading Edge Erosion

Wind turbines are a low-cost, low-carbon electricity generation source and thus an effective means to reduce climate forcing [1,2]. Accordingly, the global wind energy installed capacity passed 1 TW in 2023 and is projected to surpass 2 TW before 2030 [3]. In the United States of America (USA), wind turbines contributed over 450 TWh of electricity to the grid (over 10% of national consumption) in 2023 [4] from an installed capacity of approximately 150 GW [3].

The efficiency of electricity generation, as measured using capacity factors (ratio of annual energy production (AEP) to maximum AEP of all wind turbines operated at their rated capacity all of the time), for wind turbines installed in the USA between 2009 and

2020 increased from 0.29 to 0.41 [5]. This is due in part to increasing wind turbine rated (or nameplate) capacity [6] and wind turbine dimensions, including rotor diameter, which increases the blade tip speed [7].

The levelized cost of energy (LCoE) from a generation source is given as follows:

$$\text{LCoE} = \frac{\sum_{n=1}^i (\text{CAPEX}_n + \text{O\&M}_n) / (1 + r)^n}{\sum_{n=1}^i \text{AEP}_n / (1 + r)^n} \quad (1)$$

where CAPEX_n = capital expenditures in year n , O\&M_n = operations and maintenance costs in year n , AEP_n = annual electricity production in year n , where $n = 1$ to i , where i is the lifetime, and r = discounting rate.

Inflation-adjusted LCoE in USD 2020/MWh from wind installations in the USA approximately halved between 2009 and 2020 [8], in part due to reductions in O&M costs [8]. Future O&M cost estimates are uncertain, but there is evidence that they are an increasing component of LCoE [9].

Wind turbine blades are multi-layered, comprising an outer coating layer that is designed to protect the underlying glass fiber (or carbon fiber)-reinforced polymer that is applied to a load-carrying shell [10]. Blade integrity is essential to efficient electrical power generation from wind turbines (AEP) and blades significantly contribute to both overall purchase price (>20% of CAPEX, [11]) and O&M costs [12,13]. During 2019, global O&M costs for onshore wind farms exceeded USD 15 billion with over half of expenditures being on unplanned repairs [14]. Past research has reported blade damage as the major cause of wind turbine failures [15]. A sample of 5800 wind turbine failure events during 1993 and 2006 found blade repairs typically took between 260 and 340 h [16]. One analysis found that “preventive maintenance could reduce the average lifetime maintenance cost 11.8 times comparing the corrective maintenance for wind turbine blades” [17].

An important cause of blade damage and degraded aerodynamic performance is leading edge erosion (LEE) [18]. LEE involves material loss of blade coatings, leading to exposure and loss of the glass fiber laminate. The resulting roughening of the blade [19] reduces lift and increases drag, leading to reduced power production (AEP) [20–24]. Accordingly, a range of techniques have been proposed to more efficiently detect blade damage to inform possible repair [25,26], and a number of research projects have been initiated to predict and reduce LEE [18]. The issuance of testing standards for erosion resistance of leading edge protective (LEP) products by Det Norske Veritas (DNV) in 2020 further emphasizes the importance of LEE to the wind energy industry [27].

Recent research on indicative costs for repair of LEE as a function of damage severity report ranges (for 3 blades) from GBP 7000 for minor damage (categories 1–2, discoloration of coating to removal of up to 10 cm² of coating) to GBP 42,000 for major damage (category 4, coating removed and partial removal of first layer of laminate, resulting in AEP losses of 3%) to GBP 3,750,000 (category 5, holes in laminate, loss of AEP ≥ 5%) [28] (estimated AEP loss as a function of damage severity from [19]). While relatively few wind farm owner-operators have released information regarding the extent or timing of LEE emergence, according to one report when EDP Renewables inspected 201 rotor blades on a wind farm after 14 years of operation, 174 blades (87%) had visible signs of erosion, and 100 blades (50%) showed severe LEE [29]. Further, an analysis of wind turbine blades from India found evidence of LEE in as little as two years of operation [30]. Slowing/mitigating coating failure and LEE and thus extending blade lifetimes has the potential to contribute further reductions in LCoE from wind turbines via both increased AEP and reduction of O&M costs and may aid in partially alleviating cost/environmental issues linked to recycling/disposal of blades [31].

LEE is primarily the result of material stresses induced when hydrometeors (i.e., rain droplets, hail stones) impact on rapidly rotating blades [32–36]. Experimental data and detailed modeling using finite element methods indicate that the impact force and von Mises stresses in coatings for individual hydrometeor impacts scale with impact velocity and hydrometeor mass and hence diameter [37–39]. Hence, impacts from larger hydrometeors lead to coating failure with fewer impacts per unit area because they have higher kinetic energy of impact and induce both larger stress values at the impact site and stress waves that travel further through the material [39]. Therefore, the cumulative material stresses in blade coatings from hydrometeor impacts are amplified under the following conditions:

- Under high wind speeds when closing velocities (v_c) between the hydrometeors and the rotating blade are maximized. v_c is typically dominated by the blade tip speed (Figure 1a) which exceeds the terminal fall velocity (v_t) of hydrometeors (Figure 1b) frequently by an order of magnitude.
- During periods of intense precipitation when there are many, and larger, hydrometeors [38] (Figure 1c) and/or during periods of hail.

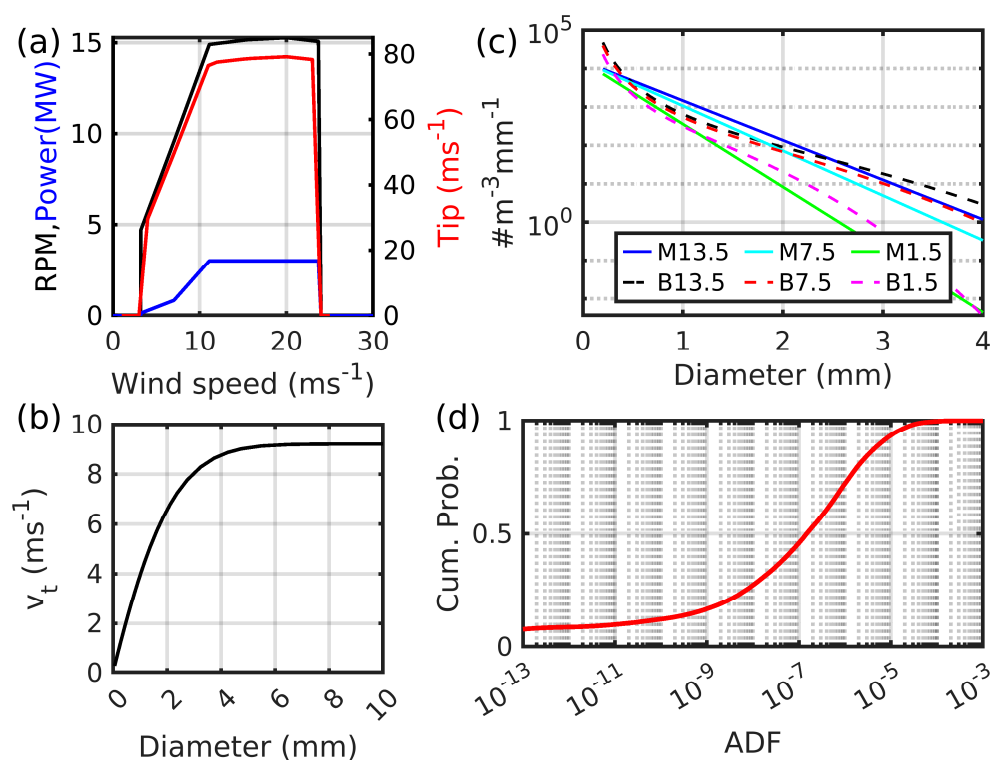


Figure 1. Overview of parameters that dictate wind turbine blade leading edge erosion. (a) Rotor rotational (RPM, black) and tip (Tip, red) speed and electrical power generation (Power, in MW, blue) as a function of the hub-height wind speed for the 3 MW WINDPACT reference wind turbine [40]. (b) Terminal fall velocity (v_t) as a function of hydrometeor diameter [41]. (c) Number density of rain droplets ($\# \text{m}^{-3}$ per mm of diameter space) computed using the Marshall–Palmer distribution approximation (prefix M) [42] and the approximation of Best [43] (prefix B) for three different rainfall rates (in mmhr^{-1}). (d) Cumulative density function (CDF) of 1-min blade coating accumulated distance to failure (ADF) values computed using the Springer model [44,45] and 4 years of hydrometeor size distribution and wind speed measurements from the US Department of Energy’s Atmospheric Radiation Measurement (ARM) experimental station in the Southern Great Plains (location shown in Figure 2a by the magenta dot, see details in [46]).

Most wind turbines in the contiguous USA (CONUS) are deployed in locations with good wind resources, but also where hydroclimatic conditions associated with highest

material stresses and hence LEE potential are frequent (heavy precipitation and hail during periods with high wind speeds; thus, turbines are operating at maximum rotational speed) [35] (Figure 2a–c). Further, wind turbines being deployed offshore are physically larger and have both longer blades and higher tip speeds than those deployed onshore [3]. This leads to higher closing velocities with falling hydrometeors and thus potentially more rapid erosion in offshore locations that also have higher O&M costs [47] and are also experiencing pricing challenges linked to risk and cost of capital [48].

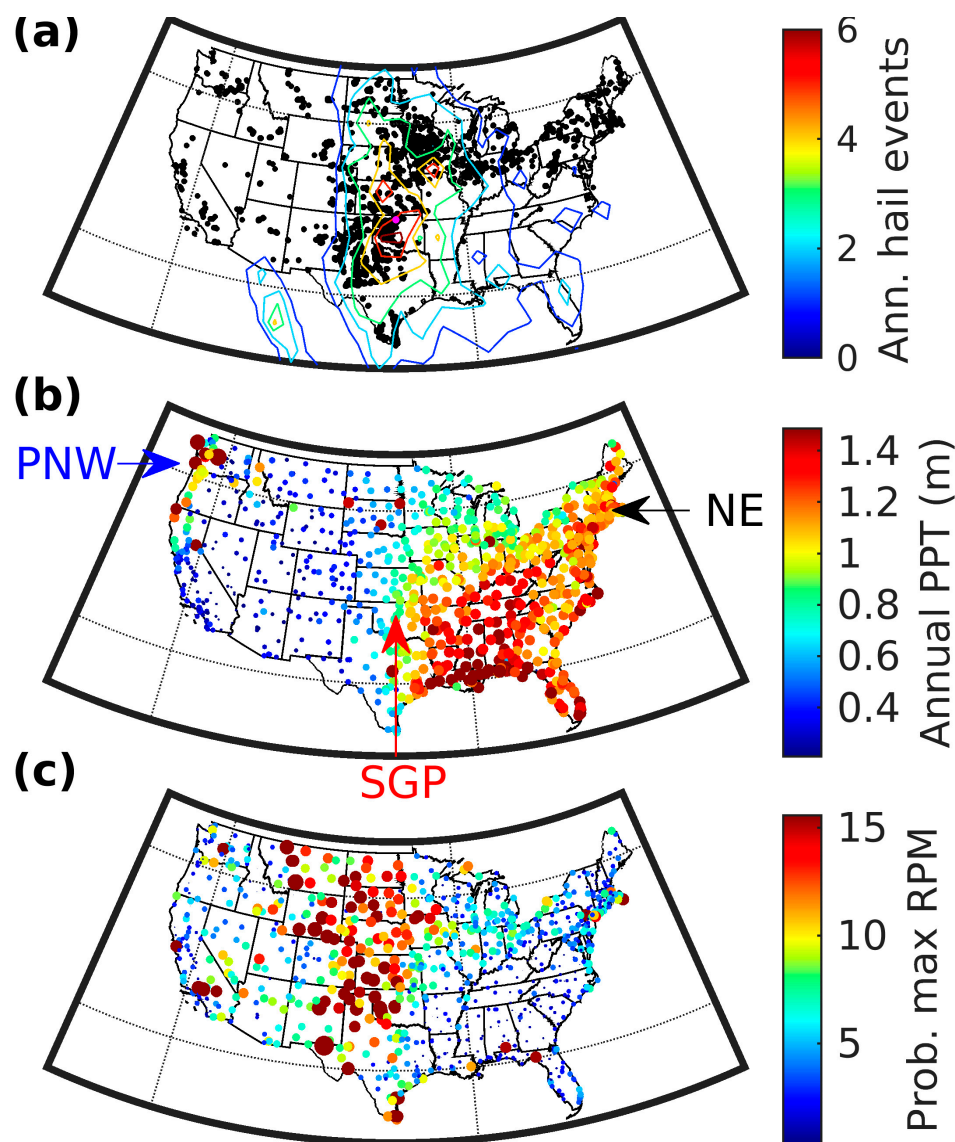


Figure 2. Overview of datasets. (a) Wind turbine locations in the CONUS at the end of 2023 based on data from the USGS Wind Turbine Database [49,50] (black dots). The magenta dot shows the location for which blade coating ADF estimates are shown in Figure 1d. Contours show estimated annual hail frequency from the NASA Passive Microwave Hail Climatology Data Products V1 dataset [51]. (b) Annual total precipitation at the Automated Surface Observing Station (ASOS) sites computed using 1-min observations from 2005 to 2022. (c) Probability that the wind speed at the hub height (90-m) of the 3 MW WINDPACT reference wind turbine is in the range with maximum rotor rotational speed (RPM, Figure 1a) based on ASOS observations to 10-m height and application of the power law (see Equation (2)). The arrows and text (PNW, SGP, and NE) in frame (b) show the locations used to illustrate the time series of ADF. Color bar limits in (b,c) are set to 5th to 95th percentile values to aid legibility of spatial gradients.

Options for reducing wind turbine blade LEE include the following:

- (i) Redesign of blades, use of more energy absorbing materials in coatings or reduction of manufacturing defects [52–54]. These may increase manufacturing, and hence CAPEX costs, and they can only be applied to new wind turbines.
- (ii) Use of leading edge protection (LEP) products [55,56]. The application of LEP as part of the blade manufacture or after wind turbine deployment will increase CAPEX or O&M costs, respectively. Use of LEP may also negatively impact blade aerodynamics, resulting in reduced AEP [21,57,58].
- (iii) Dynamical operation of wind turbines to reduce rotor speed during periods associated with high material stresses (i.e., intense precipitation at high operating wind speeds) [32]. This erosion-safe mode operation necessarily reduces AEP due to the loss of electricity production during curtailment/deregulation to slow rotor speeds, but may decrease O&M costs by increasing blade coating lifetimes, leading to a net benefit in terms of LCoE [46].

Cost–benefit analyses designed to select between options (ii) and (iii) for a given environment are critically reliant on modeling using the joint probability distributions of wind speeds and hydroclimate properties that dictate material stresses in blade coating and LEE.

The ASOS observations used in the current analysis illustrate the presence of marked geospatial variability in annual total precipitation (Figure 2b) and the frequency with which wind turbines are likely to have their blades rotating at the maximum speed (Figure 2c). There is, therefore, an expectation that wind turbine blade coating lifetimes will equally exhibit high spatial variability across North America. No comprehensive geospatial description of blade coating lifetimes is currently available for the CONUS, but past research using wind speeds and precipitation estimated from six National Weather Service RADARs demonstrated very high spatial variability in precipitation-induced blade coating damage potential and indicated the importance of low-probability, high-impact events to cumulative annual total kinetic energy transfer [36]. Analyses for a site in the Southern Great Plains (SGP) region of the USA also showed that the probability distribution of high-frequency accumulated distance to failure (ADF) of blade coatings due to hydrometeor-induced stresses is extremely heavy tailed. That is, when ADF estimates are derived using the Springer model applied to 1-min resolution hydrometeor size distribution and hub-height wind speed measurements, relatively few 1-min periods dominate the accumulation of material stress (Figure 1d) and hence the duration of time required for onset of erosion (when $ADF = 1$) [46].

In analyses of data from the SGP where total ADF is dominated by a few time periods, modeling using rotor-speed curtailment during the most erosive 0.1–0.2% of 10-min periods (i.e., enactment of option (iii) erosion-safe mode) was found to substantially increase blade coating lifetimes and thus lead to a minimized LCoE despite the associated loss of power production and hence revenue [46]. Conversely, in a situation where ADF increments occur in more numerous and more evenly weighted periods, option (ii) may be preferable in terms of net impact on LCoE. Selecting between options (ii) and (iii) will necessarily depend on the cost of blade repair, purchase of LEP products, and their deployment costs [28], as well as quantification of the amount of time when erosion-safe mode operation is required and, thus, how much AEP is sacrificed. Hence, market conditions, such as the purchase price of electricity, which exhibits marked variations in time and space, must also be considered [59,60]. For this reason, it is useful, as herein, to quantify not only wind turbine blade coating lifetimes but also the frequency of periods that cause large material stress (ADF increments) and the seasonality of these highly erosive periods. Such information can

facilitate economic modeling by wind farm owner operators to select the most appropriate LEE mitigation approach in each location.

1.2. Objectives

Our primary objective is to develop and present the first geospatial description of wind turbine blade coating lifetime and hence LEE potential for the continental USA (CONUS) that can be used to aid in decision making for wind farm owner-operators with respect to adoption/selection of LEE mitigation measures. Importantly, the modeling presented herein not only quantifies the duration of time prior to coating failure and erosion onset but is also used to quantify the degree to which coating ADF at each location exhibits evidence of being dominated by relatively few extreme events and their seasonality. This information is essential for costing of each LEE mitigation option at a given location.

2. Materials and Methods

2.1. Meteorological Observations

Precipitation intensity is zero-bounded, and the probability distribution is both heavy tailed and dependent on spatial and temporal resolution of the data and hence the degree of averaging [61–63]. As described above, high ADF values occur during periods of very intense precipitation and high wind speeds when many, large hydrometeors (Figure 1c) collide with a rapidly rotating blade at high closing velocities (Figure 1a,b). Hence, there is evidence that the probability distribution of high-frequency ADF increments for blade coatings may also be heavy tailed (Figure 1d). Thus, it is essential to use high-frequency meteorological data to generate wind turbine blade coating lifetime estimates and thus the expected duration of time prior to LEE.

The full research methodology applied in this work is detailed below with a schematic workflow also given in Figure 3. The first step is to describe the prevailing meteorological conditions at each location. To do so, we use records from 883 National Weather Service (NWS) Automated Surface Observing System (ASOS) network stations, covering the period from 2005 to 2022. These records include 1-min accumulated precipitation plus 2-min sustained wind speed within a 5-min period. The ASOS network is subject to stringent site selection [64], instrument maintenance [65], and data quality assurance protocols [66]. Sustained wind speed measurements at 10-m height are obtained using a heated 2D sonic anemometer [67]. They are reported herein in ms^{-1} , but are recorded in whole knots with values below 3 knots reported as 0 [68]. Accumulated precipitation measurements are taken using a heated and wind-shielded tipping bucket rain gauge [69,70]. The minimum 1-min precipitation depth is 0.01 inch (0.254 mm) and is equal to one tip of the pivoted bucket within the rain gauge. One-minute accumulated precipitation is aggregated to 5-min periods for which wind speeds are reported and converted to a rainfall rate in mmhr^{-1} . Blade coating lifetime statistics presented herein are corrected for missing data periods to generate an effective 18-year blade coating ADF. Three of the 883 ASOS stations have <50% of possible observations available and are excluded from further analyses.

The WINDPACT reference wind turbine [40] used in this analysis to derive 5-min time series of blade rotational speed as a function of prevailing wind speed (Figure 1a). This wind turbine has a rated capacity of 3 MW and hub height of 90-m and thus is a reasonable representation of the average of the current US wind turbine fleet [4]. ASOS wind speeds as measured at 10-m (WS_{10}) are scaled to the hub height of 90-m (WS_{90} , referred to here as WSHH) using the power law and a coefficient of $1/7$ [71]:

$$WS_{90} = WS_{10} \times \left(\frac{90}{10}\right)^{1/7} \quad (2)$$

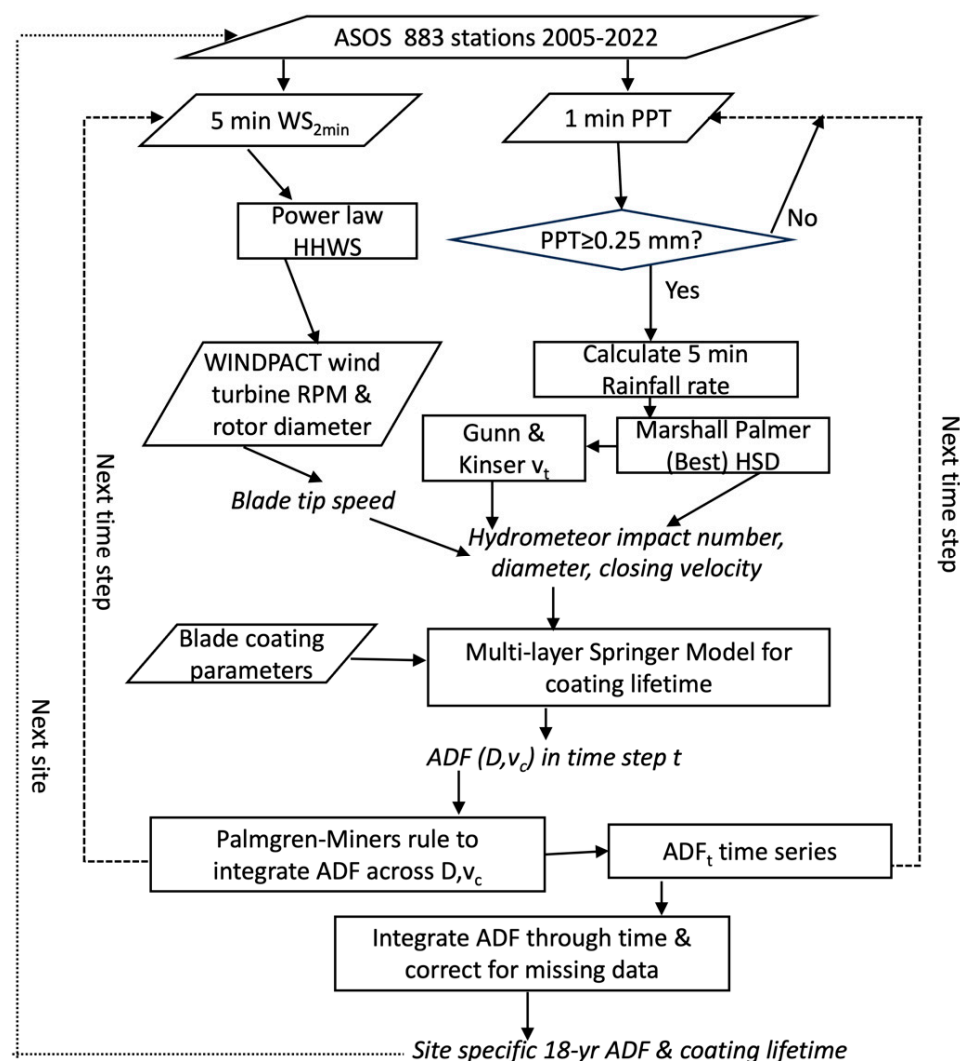


Figure 3. Flowchart presenting the workflow used to create a time series of 5-min blade coating accumulated distance to failure increments ($ADFi_t$), 18-year ADF and blade coating lifetimes for each site.

Thus, the scaling factor applied to the ASOS 5-min interval wind speed measurements for use in determining the blade rotational speed and tip speed is 1.38.

To illustrate variations in 5-min coating ADF increments as derived using the ASOS measurements and the Springer model in different climates and regions of the CONUS, we present data from indicative stations in the Pacific Northwest (PNW) from KAST in Astoria, Oregon; Southern Great Plains (SGP) from KOKC in Oklahoma City, Oklahoma; and the Northeast (NE) from KACK in Nantucket, Massachusetts. These locations are close to major wind turbine deployments (Figure 2a). The PNW experiences high annual total precipitation (Figure 2b). The SGP has the greatest concentration of wind turbines and an extreme hydroclimate with a high frequency of deep convection and intense precipitation [72,73] (Figure 2a,b). The NE site is selected to be close to the US eastern coastline and hence adjacent to areas where major offshore wind energy installations are currently underway [74].

2.2. Mapping Atmospheric Drivers to Damage

Multiple engineering models have been developed to simulate the material stresses induced by hydrometeor collisions with the wind turbine blade that cause coating degradation and lead to blade LEE [38,75,76]. Herein, we employ a multi-layer version of the

Springer model [44,45,77–79] that uses the material properties of the blade and coating to compute the number of impacts required for failure per unit area (N_i , m^{-2}) for a given hydrometeor diameter (D , m), impact velocity (v_c , ms^{-1}), and impact angle (θ). Using the integration of hydrometeor diameter, closing velocity, and then time, the model can be used to derive an accumulated distance to failure of the coating and hence onset of blade erosion. The Springer model has been widely described and validated relative to rain erosion tests [78] and is also employed within the recommended practice (RP) for evaluation of erosion and delamination for leading edge protection systems of rotor blades issued by DNV [27].

The fundamental equations of the Springer model are presented below. A range of coefficient values have been postulated to represent wind turbine blade materials [79]. Hence, the values of the model coefficients used in the current research are given below along with the reference from which the values are drawn.

$$N_i = \frac{4\pi}{D^2} a_1 \left(\frac{S_{ec}}{\sigma_0} \right)^{a_2} \quad (3)$$

where S_{ec} = erosion strength of the coating. In addition, a_1 and a_2 are constants that in the current implementation of the model have values of 7×10^6 and 5.7, respectively [79]. Here, σ_0 = average stress of the coating surface, and scales with the thickness of the coating, the coating and substrate material properties, and the hydrometeor diameter and is expressed as follows:

$$\sigma_0 = v_c \frac{Z_L \cos(\theta) (\psi_{sc} + 1)}{\left(\frac{Z_L}{Z_c} + 1 \right) (1 - \psi_{sc} \psi_{Lc})} \left(1 - \frac{(1 - e^\gamma) (\psi_{Lc} + 1) \psi_{sc}}{\gamma (\psi_{sc} + 1)} \right) \quad (4)$$

where v_c = impact velocity (set as the closing velocity between the hydrometeor and the blade); θ = impact angle between the hydrometeor and the blade (assumed here to be 0, i.e., there is no deflection of the hydrometeor and the impact is normal to the leading edge [79]); Z_x = impedance of each material; and $\rho_x C_x$, where ρ_x = material density. In the following, subscripts (x) are used to refer to L = liquid, c = coating, and s = substrate. Here, ρ = material density: $\rho_c = 1690 \text{ kgm}^{-3}$ [78], $\rho_L = 997 \text{ kgm}^{-3}$ [79] and $\rho_s = 1930 \text{ kgm}^{-3}$ [78]. C = elastic wave speed: $C_L = 1481 \text{ ms}^{-1}$ [79], $C_c = 1730 \text{ ms}^{-1}$ [78,79] and $C_s = 2390 \text{ ms}^{-1}$ [78]. ψ_{xx} = relative acoustic impedance, where sc = substrate coating and Lc = liquid coating.

$$\psi_{sc} = \frac{Z_s - Z_c}{Z_s + Z_c} \quad (5)$$

$$\psi_{Lc} = \frac{Z_L - Z_c}{Z_L + Z_c} \quad (6)$$

Here, γ = coating thickness parameter (maximum number of reflections during the impact time within the coating thickness) and is expressed as follows:

$$\gamma = \frac{2C_c Z_c (Z_L + Z_s) D}{C_L (Z_c + Z_L) (Z_c + Z_s) h} \quad (7)$$

where h = coating thickness. A range of blade coating thicknesses are reported in the literature. For example, values of 100 to 3000×10^{-6} m are given in [75]. Increasing the coating thickness reduces the number of stress reflections at the coating/substrate boundary. Thus, for given substrate impedance, the ratio $\frac{S_{ec}}{\sigma_0}$ and hence the number of impacts to

failure from Equation (3) are minimized for high D to h ratios [75]. In the current research, h is set to 750×10^{-6} m [79].

$$S_{ec} = \frac{4(b_c - 1)\sigma_{Uc}}{(1 - 2\nu_c)\left(1 - \left(\frac{\sigma_{Ic}}{\sigma_{Uc}}\right)^{b_c - 1}\right)(2k|\psi_{sc}| + 1)} \quad (8)$$

where σ_{Uc} = coating ultimate tensile strength (1.30×10^7 Pa [78]), σ_{Ic} = coating endurance limit (6.30×10^6 Pa [78]), and b_c = coating Springer fatigue knee, which is computed from the material fatigue knee (b_{2c} , 16.52 [78]) as follows:

$$b_c = \frac{b_{2c}}{\log_{10}\left(\frac{\sigma_{Uc}}{\sigma_{Ic}}\right)} \quad (9)$$

where ν_c = coating Poisson ratio (0.295 [78]). Here, k is given as follows:

$$k = \frac{1 - e^{-\gamma}}{1 - \psi_{sc}\psi_{Lc}} \quad (10)$$

Palmgren–Miner’s rule is used to integrate across all hydrometeor D and closing velocities to quantify the accumulated distance to failure (ADF_t) of the blade coating in each 5-min period [78,79]:

$$ADF_t = \sum_{d=1}^{d=kk} \sum_{v=1}^{v=mm} \frac{N(d,v)}{N_i(d,v)} \quad (11)$$

where ADF_t is the accumulated distance to failure of the blade coating in time interval t; d is the hydrometeor diameter class (d = 1 to kk, where kk is the largest hydrometeor diameter class considered); v is the closing velocity class (v = 1 to mm, where mm is the largest class of closing velocity considered); $N(d,v)$ is the number of impacts in each diameter and velocity class; and $N_i(d,v)$ is the number of impacts in that diameter and velocity class to failure (see Equation (3)).

Integration of ADF_t through time is used to define the duration of time required for the accumulated number of impacts in each diameter and closing velocity class required to reach $ADF = 1$. When $ADF = 1$, this indicates the end of the incubation period where stress is accumulated by the surface, but the aerodynamic performance is virtually unaffected. $ADF = 1$ indicates the onset of erosion, mass loss from the blade, and degradation of blade aerodynamic performance. The coating lifetime in fraction of years is thus the duration of time elapsed for ADF to reach a value of 1.

The Springer model also requires information regarding the hydrometeor size distribution (HSD, hydrometeor counts in diameter classes). Herein, we employ the Marshall–Palmer approximation [42] to generate these HSDs:

$$N = \frac{N_0}{\Lambda} e^{-\Lambda R} \quad (12)$$

where N = number of droplets above radius, R (m), per cubic meter of air ($\#m^{-3}$); $\Lambda = 8200 \times RR^{-0.21}$ (m^{-1}); $N_0 = 1.6 \times 10^7 m^{-4}$; and $RR =$ rainfall rate ($mmhr^{-1}$) (Figure 1c). For comparative purposes, we also present example ADF increments based on analyses in which the HSD is computed using the approximation of Best [43]:

$$N = \frac{W}{V} \left(\frac{k_i \times D^{k_i-1}}{a^{k_i}} \right) e^{-[D/a]^{k_i}} \quad (13)$$

where N = number of droplets above diameter, D (in mm), per cubic meter of air ($\#m^{-3}$); V = droplet spherical volume (mm^3); W = total water volume ($67 \times RR^{0.846}$) (mm^3m^{-3}); $k_i = 2.25$; and $a = 1.3 \times RR^{0.232}$.

The modeling additionally requires information regarding hydrometeor fall velocity to estimate the closing velocity with the rotating blade. Herein, we use the terminal fall velocity (v_t) as a function of hydrometeor diameter from Gunn and Kinzer [41] (Figure 1b). The closing velocity (v_c) in each time step (t) and for each diameter (D) is a function of the terminal fall velocity (v_t) for that of a hydrometeor of a given diameter, horizontal wind speed at hub height (WSHH), linear speed of the blade tip (v_r), and blade position (ϕ):

$$v_c(D, t, \phi) = \left[WSHH^2 + (v_r + v_t(D) \times \cos\phi)^2 \right]^{1/2} \quad (14)$$

Thus, if $WSHH = 16 \text{ ms}^{-1}$, the blade tip speed is 78.7 ms^{-1} , and a 2 mm diameter hydrometeor falling at a v_t of 6.55 ms^{-1} will have a closing velocity with the blade that varies between 73.9 and 86.7 ms^{-1} depending on the blade position.

The total number of impacts of hydrometeors of a given diameter (D) on the blade leading edge during time interval t ($I(D, t)$), also known as the impact rate, is a function of the hydrometeor number density ($N(D)$) as described using Equations (12) or (13) and their closing velocity from Equation (14):

$$I(D, t) = N(D) \times v_c(D, t, \phi) \quad (15)$$

Five-minute rainfall rates (in $mmhr^{-1}$) and WSHH from ASOS observations are not continuous but rather take discrete values. Hence, a matrix of ADF values as a function of 41 WSHH values (0 to 40 ms^{-1}) and 51 RR values (0 to 150 mmhr^{-1}) was computed. This matrix comprises a look-up table (LUT) that is applied to time series from each ASOS station to determine the ADF increment (summed across all D) for every 5-min record of wind speed and rainfall rate (ADF_t). Summing the time and correcting for missing data periods, an effective 18-year blade coating ADF is computed for each ASOS location.

Two statistical metrics are presented to describe the concentration of coating ADF increments in time: (a) sum of the top n values from each time series of 5-min ADF_t , where n varies from 1 to 1000, and (b) probability that consecutive periods will exceed a specified ADF threshold. The frequency of occurrence of high ADF_t is also presented by computing the number of occurrences of $ADF_t > 1 \times 10^{-4}$ in each calendar month divided by the total number of observations in that month.

The heavy-tailed nature of the probability distributions of ADF_t has the implication that relatively long records of meteorological drivers are required to generate robust 18-year ADF and hence blade lifetime estimates at each site. To examine the importance of data record duration and the precise years present in the record, a resampling analysis using complete years is performed. In this analysis, 18-year ADF is computed using record lengths of 1 to 17 years with sampling of individual calendar years without replacement.

Confidential communication with a major wind farm owner-operator indicated that they purchase estimates of total annual precipitation and mean wind speed to provide preliminary information regarding the duration of time to coating failure at prospective development sites. Hence, a final analysis is performed to evaluate the degree to which the spatial variability in 18-year ADF can be explained by these variables. This analysis leverages linear regression with parameter fitting using maximum likelihood estimation.

3. Results

3.1. Simulated Blade Coating Lifetime as a Function of Prevailing Meteorology

Figure 4a presents a heatmap of 5-min accumulated distance to failure (ADF_t) for blade coatings, integrated across all hydrometeor diameters for example combinations WSHH and RR where the number concentration of hydrometeors of each diameter is computed using the Marshall–Palmer approximation. While the absolute values of 5-min ADF increments are naturally dictated by the coefficients used in the Springer model, this heatmap illustrates several key points. First, based on the multi-layer Springer model, hydrometeors associated with RR of 15 mmhr^{-1} , across all wind speeds and hence rotor speeds, are >6 times as efficient at causing material stresses, and contributing to ADF increments, than those associated with a RR of 1.5 mmhr^{-1} . Second, because the closing velocity between the hydrometeors and the blade is highly dependent on the rotational rate of the wind turbine blades, periods when the WSHH is at, or close to, the inflow wind speed with maximum RPM are particularly important to the ADF . For a RR of 4.5 mmhr^{-1} , there is 50-fold higher 5-min ADF increment when wind speeds are 16 ms^{-1} versus 3.25 ms^{-1} . Third, accurate specification of the frequency of conditions in differing rain rate and wind speed classes is critical to determining ADF of wind turbine blade coatings and hence the likelihood of LEE in a given time interval. Finally, the approximation applied to compute the HSD plays a role in the absolute values of blade coating ADF for a given rain rate and wind speed (cf. Figure 4a,b). ADF is larger when the HSD is computed using the formulation of Best (Equation (13)) versus that of Marshall–Palmer (Equation (12)). Thus, coating lifetimes would be shorter if the Best HSD were applied. For the example WSHH and RR illustrated in Figure 4, the ratio of ADF increments from calculations using Best versus Marshall–Palmer range from 2.52 for low rainfall rates (1.5 mmhr^{-1}) to 1.43 for high rainfall rates (15 mmhr^{-1}).

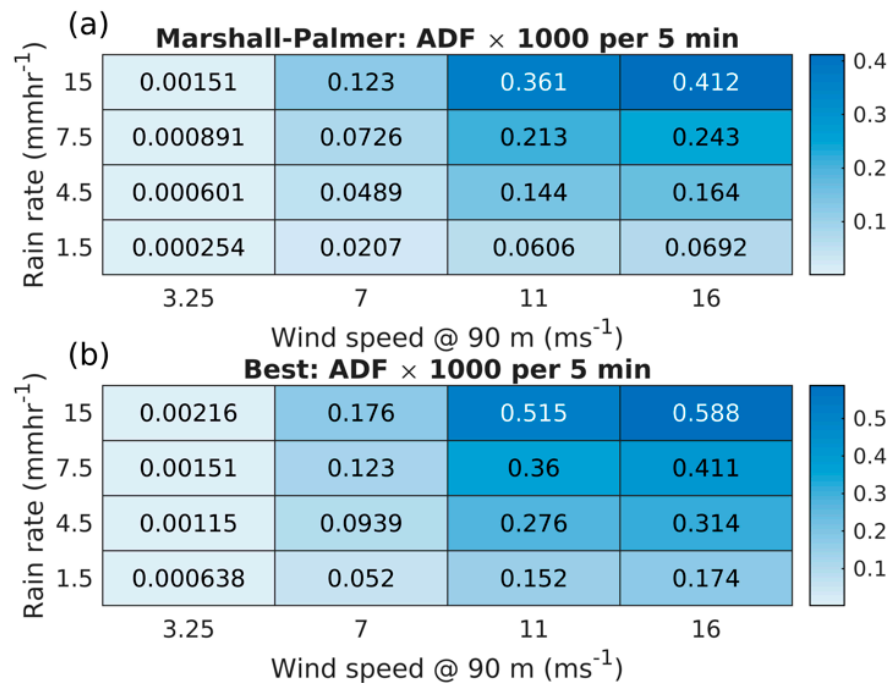


Figure 4. A heatmap of blade coating ADF_t ($\times 10^3$ to aid visibility) for 5-min periods with example wind speeds and rainfall rates. ADF_t computed using (a) HSD from Marshall–Palmer and (b) HSD from Best. ADF_t is computed using the Springer model, the closing velocity derived using the WINDPACT 3 MW reference turbine and hydrometeor, and v_t from Gunn and Kinzer [41].

3.2. Geospatial Variability of Blade Coating Lifetime

In accord with a priori expectations and limited past research [36], the blade coating lifetime estimates across the CONUS exhibit marked geospatial variability. Here, 18-year ADF estimates range from <0.1 at the ASOS sites with the least erosive climate to a maximum of 4 (Figure 5a). A value of 4 indicates that a blade coating with the material properties employed in the Springer model is projected to fail 4 times during an 18-year period. Alternatively stated, the blade coating is expected to fail, on average, in just over 4 years. Analyses for one-quarter of the ASOS stations indicate an 18-year $ADF > 1$, and two-thirds of sites have a $ADF > 0.5$. Stations with 18-year $ADF > 1$ that are close to current wind turbine installations (Figure 2a) are clustered along the US west coast, in the Central Plains, and along the US east coast (Figure 5a). Several sites exhibit blade coating lifetimes of <12 years (Figure 5b). The site with the highest 18-year ADF (4) is KCEC in Crescent City, California. This coastal station experiences high annual total precipitation (1539 mm) and a relatively high frequency of precipitation during periods when the wind speed is such that the reference wind turbine would be operating at high RPM.

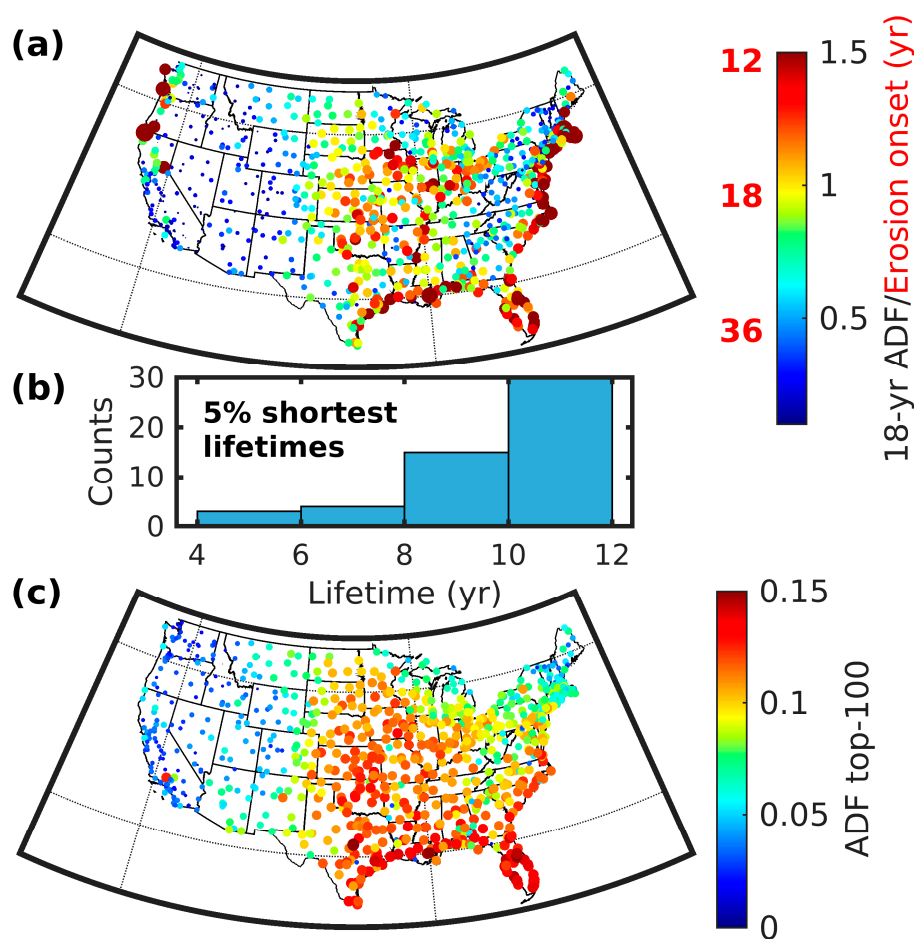


Figure 5. Blade coating lifetimes. (a) Eighteen-year accumulated distance to failure (ADF) and coating lifetime (erosion onset time in years) at each of the ASOS sites. A value of 1 indicates that the coating lifetime has been exhausted in 18 years, and blade damage is predicted to have commenced. (b) Histogram of the coating lifetimes for the top 5% of ASOS sites with the highest 18-year ADF (i.e., 18-year $ADF > 1.5$). (c) The ADF from the top 100 most erosive 5-min periods during the measurement record. Color bar limits in panels (a) are set to 5th to 95th percentile values to aid legibility of spatial gradients.

Data regarding the need for blade repair or LEP application are generally kept confidential by wind farm owner-operators. Thus, it is difficult to evaluate the coating lifetime

predictions presented in Figure 5a. An earlier analysis using independently measured HSD and fall velocities from a disdrometer and wind speeds from a lidar at the US Department of Energy Atmospheric Radiation Measurement (DoE ARM, see location in Figure 2a) site in Lamont, Oklahoma predicted the 3 MW reference turbine would experience coating failure in slightly over 16 years (see cumulative density function of 1-min ADF increments from that analysis in Figure 1d) [46]. Analyses presented herein for an ASOS site 32 km from the ARM location are consistent with that earlier work and indicate an ADF of 1 over the 18-year period (i.e., a coating lifetime of ≤ 18 years).

3.3. Temporal Variability in Blade Coating Lifetime Reduction

The probability distributions of 5-min ADF increments varies markedly across the USA. Accordingly, the contribution of the top 100, 5-min periods in terms of incremental contributions to ADF also exhibits marked spatial variability (Figure 5c). Over much of the western half of the CONUS, the top 100 most erosive 5-min periods contribute less than 5% of the total 18-year ADF, and $<5\%$ of a blade coating lifetime. In other locations, for example much of the SGP, values exceed 0.1, indicating that 10% of the coating lifetime may be exhausted during as few as 100 5-min periods. The top 100 5-min ADF values along the Gulf coast of the CONUS (i.e., the southeastern USA) are also very high likely due, in part, to torrential rain and high wind speeds associated with land-falling tropical cyclones [80,81].

Analyses of modeled time series from three example ASOS stations with 18-year ADF > 1.5 that are located close to major wind turbine installations indicate marked variations in the degree to which the ADF time series is heavy tailed (Figure 6a).

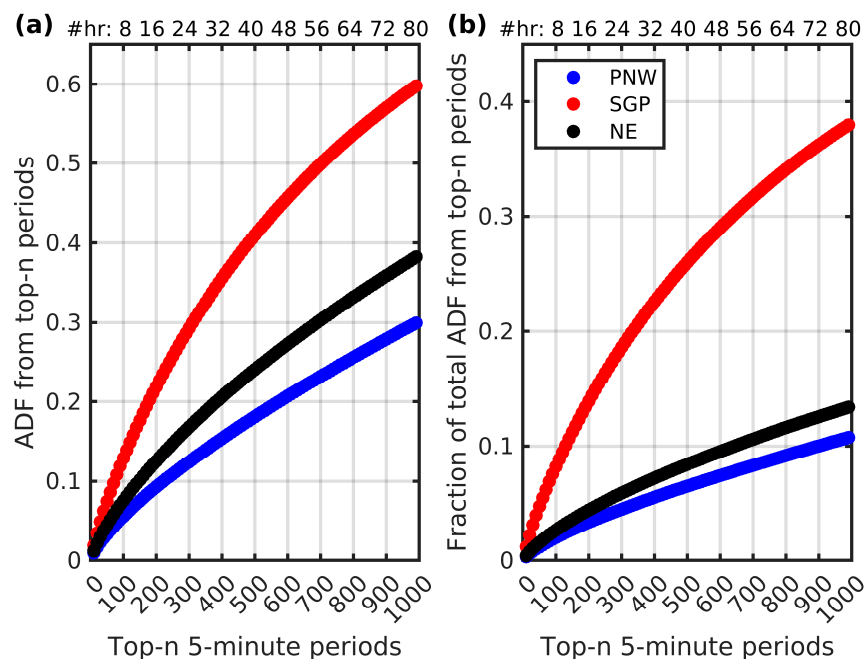


Figure 6. Concentration of blade coating accumulated distance to failure (ADF) in time. (a) ADF increment during the top-n most erosive 5-min periods (top axis = equivalent number of hours) at three example sites where 18-year ADF exceeded 1.5. (b) Fraction of total 18-year ADF contributed by the top-n most erosive 5-min periods (top axis = equivalent number of hours) at three example sites where 18-year ADF exceeded 1.5. Pacific Northwest (PNW) reports data from KAST in Astoria, Oregon (18-year ADF of 2.8). Southern Great Plains (SGP) reports data from KOKC in Oklahoma City, Oklahoma (18-year ADF of 1.6). Northeastern US (NE) reports data from KACK in Nantucket, Massachusetts (18-year ADF of 2.9) (see site locations in Figure 2).

The SGP site achieves an ADF of 0.33 (i.e., one-third of blade coating lifetime expended) in just 360 5-min periods (or 30 h) (Figure 6a). For the PNW site, 1130 5-min periods are required to achieve an ADF of 0.33. For the NE station, 790 5-min periods are required. Thus, approximately three times as many 5-min periods are required in the PNW to achieve the same accumulated level of material stress as the top 360 periods in the SGP. The dominance of a few extremely erosive periods in determining overall total 18-year ADF across these sites is even more marked (Figure 6b). Over one-third of the total 18-year ADF at the SGP site is associated with ADF increments in just 1000 5-min periods or just over 80 h (Figure 6b). This implies that there may be the greatest value in the use of erosion-safe mode in the SGP, given that curtailment of electricity production will be required during only a small number of hours each year. Conversely, for the PNW site, only just over 10% of the 18-year ADF is accumulated in the top 1000 most erosive 5-min periods.

The likelihood of highly erosive periods (5-min ADF increments of $> 1 \times 10^{-4}$) in SGP is maximized during April–June (Figure 7a) likely due to the prevalence of deep convection during these months and the associated occurrence of high rainfall rates [73]. Thus, the adoption of erosion-safe mode to extend blade lifetimes would likely be most frequent during the spring and early summer, before the peak electricity demand, which occurs during July and August in Oklahoma (data from the US Energy Information Administration (EIA) <https://www.eia.gov/>, accessed on 2 November 2024). Highly erosive periods in the PNW are confined to winter during the season of strongest synoptic-scale storms [82] and highest electricity demand (data from EIA). Highly erosive periods are more evenly distributed across all calendar months in the NE, but peak in late fall early winter, which is displaced from the summer peak in electricity demand (data from EIA) (Figure 7a).

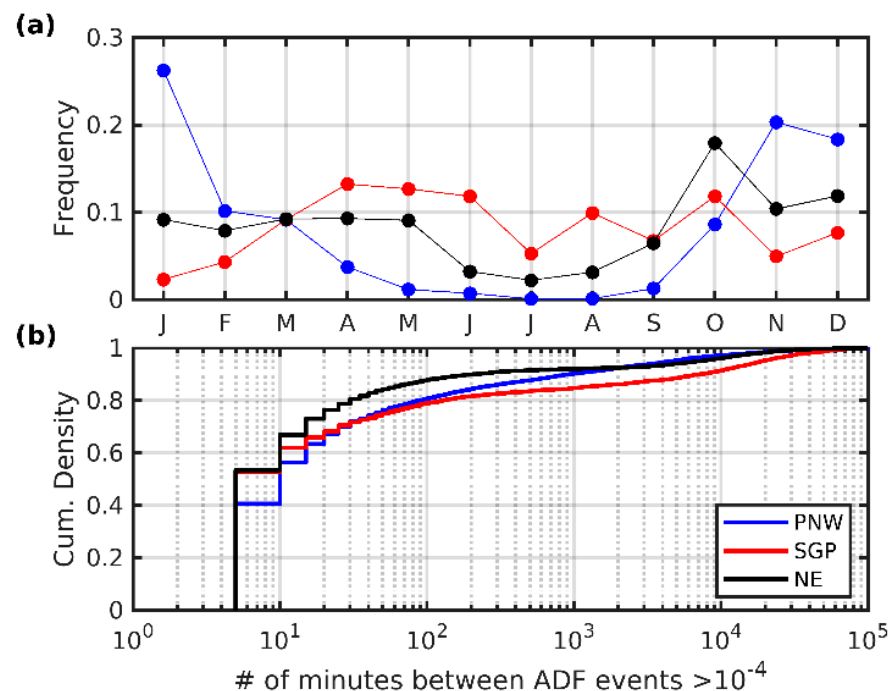


Figure 7. Temporal variability of blade coating accumulated distance to failure increments ($ADFi$). (a) Seasonality of occurrence of 5-min $ADFi$ increments $> 1 \times 10^{-4}$ and (b) the cumulative density function (CDF) of the time interval between consecutive periods with 5-min $ADFi$ increments $> 1 \times 10^{-4}$ for the exemplar sites in the Pacific Northwest (PNW), Southern Great Plains (SGP), and Northeastern US (NE) (see site locations in Figure 2b).

An additional matter of importance for the possible use of erosion-safe mode to reduce LEE is the concentration of highly erosive periods in time. Over half of periods

with ADF increments $> 1 \times 10^{-4}$ at the SGP and NE occur in consecutive 5-min periods (Figure 7b). Run length statistics suggest that 99% of time periods with continuous ADF increments $> 1 \times 10^{-4}$ have durations in the SGP of less than one hour. This implies that substantial increments in total coating ADF are contributed not only by relatively few 5-min periods, but also by those periods being highly concentrated in time. This finding would suggest a very high economic value in short-term meteorological forecasting of highly erosive events to inform decisions regarding the implementation of erosion-safe mode and hence derating of wind farms to extend blade lifetimes. It also suggests high economic value in on site measurements of precipitation characteristics in addition to wind speeds in site pre-construction assessments.

In accord with expectations, 18-year ADF computed using larger numbers of years of meteorological observations increasingly converge on best estimate values derived from all 18-years of data (Figure 8). Estimates of 18-year ADF, and hence blade coating lifetime, are also a function of the precise calendar years included particularly at sites where ADF_t is very heavy tailed (Figure 8b). For data records spanning 5 years, the minimum to maximum range of 18-year ADF estimates, derived using draws of different calendar year combinations, is 0.44 (PNW), 0.58 (SGP), and 0.39 (NE) of the 18-year ADF estimates derived using the entire data record (Figure 8). The blade coating lifetime for the PNW site computed using the most erosive 5 calendar years is 6.3 years, while the coating lifetime for the least erosive 5 years is 10 years. The best estimate of coating lifetime computed using the entire data record is 7.6 years. Equivalent estimates for the SGP are 9.6 (most erosive 5 years), 20 (least erosive 5 years), and 13 years (entire data record). Those for the NE site are 6.3, 8.9, and 7.5 years, respectively. For data records comprising 15 calendar years, the minimum to maximum range of 18-year ADF estimates is narrower with values of 0.12 (PNW), 0.18 (SGP), and 0.10 (NE) of estimates derived using the entire data record. This analysis affirms the value of using long-duration, high-frequency meteorological data in computing blade coating lifetime estimates particularly for sites in the SGP where ADF increments are concentrated in time.

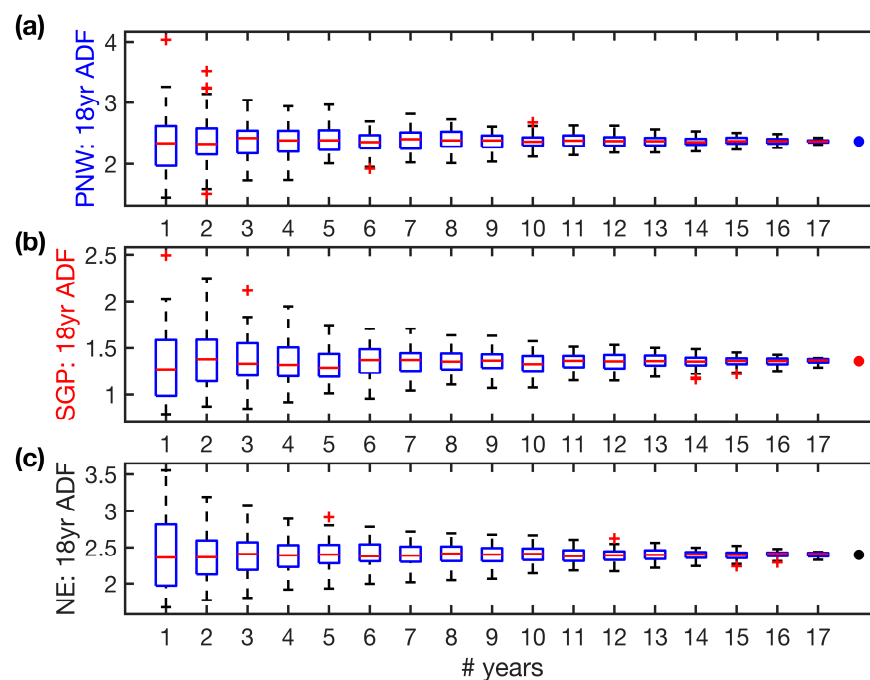


Figure 8. Boxplots of 18-year ADF estimates at (a) PNW, (b) SGP, and (c) NE ASOS stations derived using meteorological records of different durations (1–17 years). Each sample draw comprises different individual years selected without replacement. Also shown is the 18-year ADF derived using the longest record available (point at far right of each panel).

Eighteen-year ADF across the ASOS sites scales positively with both annual total precipitation and mean wind speeds (Figure 9a,b). However, consistent with the non-linear codependence of ADF on wind speed *and* rainfall rate (Figure 4) and the concentration of ADF increments in time (Figures 5b, 6 and 7b), annual mean wind speed and total precipitation are relatively poor predictors of the spatial variability of modelled 18-year ADF at sites across the CONUS. For example, 18 ASOS stations have an average annual total precipitation of 1000 ± 10 mm, and the 18-year ADF at those locations range from 0.26 to 1.33. Less than 29% of the station-to-station variance in 18-year ADF is explained by annual total precipitation, and <22% is explained by the mean wind speeds (Figure 9a,b).

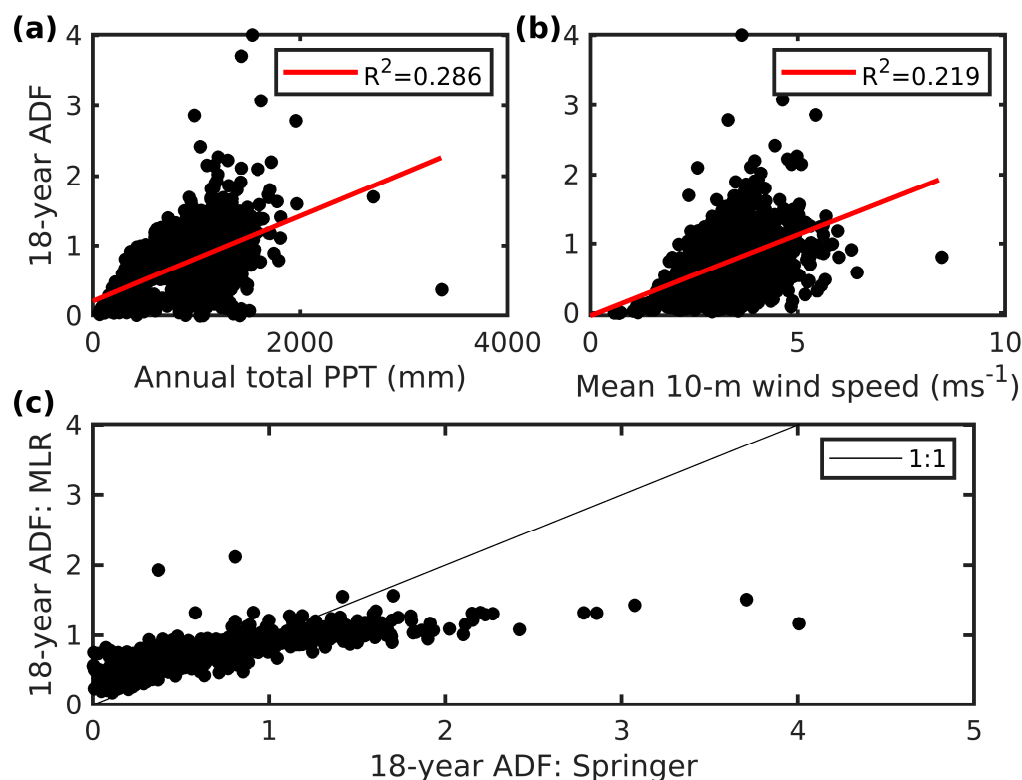


Figure 9. Relationship between blade coating lifetime and the primary meteorological drivers. Scatterplots of 18-year ADF versus (a) annual total precipitation and (b) mean 10-m wind speed at the ASOS stations. Red line indicates a linear regression fit ($18\text{yrADF} = c_0 + c_1 \times x$), where x is either annual total precipitation (PPT) or mean wind speed, and the c_0 and c_1 are the regression coefficients (all are significantly different from zero at $p = 0.01$). The variance explanation (R^2) of each of the regression fits, adjusted for sample size, is given in the legends. (c) Scatterplot of predictions of 18-year ADF derived using Equation (16) (MLR) versus the 18-year ADF at each site as derived using the detailed meteorological data and the Springer model.

A multiple linear regression model of 18-year ADF as a function of mean annual total precipitation (PPT) and a dependency on mean wind speed squared (WS^2) to capture the non-linear dependence of tip speed on wind speed (Figure 1a) with forced zero has an R^2 (variance explanation) of 0.55. In addition, the coefficients are statistically different from zero at $p = 0.01$ (i.e., 99% confidence level):

$$18\text{yrADF} = 0.0273 \times \text{WS}^2 + 5.2310^{-4} \times \text{PPT} \quad (16)$$

However, this best fit equation does not capture the dynamic range of 18-year ADF across the CONUS (Figure 8c). This analysis demonstrates the importance of using a more

mechanistic model such as Springer with high-frequency meteorological data in assessing blade coating lifetimes.

3.4. Uncertainties in Blade Coating Lifetimes

This is the first geospatial description of wind turbine blade leading edge erosion potential to be generated for the CONUS and as such represents a substantial advancement in the state of knowledge and a new tool for the wind energy industry. The atlas is publicly available and predicated on both a transparent and repeatable methodology and the use of a high-fidelity federal dataset of meteorological observations with high time resolution.

The modeled estimates of blade coating 18-year ADF, and hence likelihood of onset of blade erosion, are subject to some caveats. The resolution of the ASOS wind speed and precipitation data necessarily impacts the ADF estimates provided here. Further, as shown, the record length of the meteorological observations and the precise years sampled are also important in dictating 18-year ADF and blade lifetimes (Figure 8). Particularly, at sites with a high concentration of ADF_t in specific events, there is a need to employ long-duration time series. The absolute values of 18-year ADF are also a function of the coefficients used in the Springer model [79], and it is important to acknowledge that the coefficient values are selected to be conservative [46] and may, therefore, overestimate blade coating lifetimes. The use of alternative HSD approximations would also change the absolute values of 18-year ADF (Figure 4). However, it is likely that the spatial patterns and gradients would be substantially unchanged if different model parameters were applied. The modeling presented herein further assumes an impingement efficiency of 1 for all hydrometeor diameters. The DNV RP uses an approximation of impingement efficiency (β) as a function of hydrometeor diameter (D) that is derived from experiments in an icing research tunnel simulating icing on aircraft wings [83]. It has the following form:

$$\beta = 1 - e^{-15D} \quad (17)$$

where D is in mm. This approximation yields impingement efficiencies > 0.99 for $D > 0.3$ mm. Introduction of this correction to the number of blade impacts changes the example 5-min increments in ADF shown in Figure 4a by $<0.3\%$. Thus, corrections for impingement efficiency for smaller hydrometeors that may be deflected from the blade has a negligible impact on coating lifetimes.

The spatial variability in estimated blade coating lifetimes (described using ADF) presented here are consistent with the limited past research available for the CONUS [46]. Assessment of the reliability of this geospatial analysis would greatly benefit from the availability of data from wind farm owner-operators or wind turbine manufacturers regarding observed coating damage from their wind turbine fleets deployed across North America. While ASOS is the premier meteorological network in the USA, blade lifetime estimates derived using different models of material stress and/or meteorological datasets (observational or derived using numerical weather prediction models) would be a useful supplement to the information provided here.

An important caveat to the current research pertains to hail as a damage vector. The material's response to hail impacts is generally larger than those from rain (liquid) droplets [36,84–88]. Thus, the 18-year ADF estimates in regions such as the Southern Great Plains that have a high hail frequency (Figure 2a) [72,73] are likely to be negatively biased. With the currently available ASOS data, it is not possible to correct coating lifetimes for the potential effects of hail.

4. Concluding Remarks

Wind turbine blade leading edge erosion negatively impacts wind farm economics via decreased energy production (AEP) and increased operations and maintenance (O&M) costs. O&M costs are also a primary source of uncertainty in projections for future LCoE from wind energy [6]. While there are options to reduce LEE, the selection of an optimal solution in each location requires detailed information regarding the causes, magnitude, and spatiotemporal variability in damage accumulation. Hence, there is value in generating and applying a robust method to yield spatiotemporally explicit estimates of blade coating accumulated distance to failure (ADF) and hence erosion onset estimates.

Despite the caveats identified in Section 3.4, it is expected that the geospatial variability in relative blade coating lifetimes presented herein are relatively robust. These 18-year coating ADF estimates, computed using conservative estimates of material properties, illustrate large spatial gradients with one-quarter of locations indicating coating failure within <18 years, short of the expected wind turbine lifetime of ~30 years [89]. Many sites with high ADF estimates are in coastal locations and/or in the central CONUS, which have the highest density of wind turbine assets (cf. Figures 2a and 5).

While previous research has sought to derive estimates of wind turbine blade coating lifetimes for Danish Seas [90], northern European Seas [91], and the Netherlands [92], to the authors knowledge this is the first geospatial description of blade coating lifetimes for the USA and the first to explicitly address temporal variability of blade coating ADF increments (ADF_t). The high-frequency damage increments derived from the modeling presented here permit important insights into the relative concentration of ADF in time, the degree to which material stress is focused on consecutive periods, and the seasonality of highly erosive periods (Figures 6 and 7). This information is valuable in assessing where LEE reduction might best be achieved via adoption of erosion-safe mode and where, conversely, implementation of leading edge protective measures is economical. For regions with current/near future high densities of wind turbine installations, the ADF of blade coatings is most concentrated in time in the Southern Great Plains and is much less concentrated in time in either the Pacific Northwest or along the US east coast (Figure 6). One-third of the blade coating lifetime is expended at the SGP site during the 360 most erosive 5-min periods (or 30 h) (Figure 6). Hence, erosion-safe mode enacted during just a few minutes per year may substantially slow the progress toward coating failure and the initiation of erosion. Thus, erosion-safe mode is likely to be the most effective as a LEE mitigation measure in this region rather than incurring the cost and loss of AEP associated with the use of LEP products. Conversely, over three times as many of the highest erosive periods are required to expend 33% of the coating lifetime (i.e., achieve the $ADF = 0.33$ threshold) at the representative site in the Pacific Northwest. Hence, cost-effective solutions to elongate blade coating lifetimes in this region may involve the use of LEP products.

Author Contributions: Conceptualization, S.C.P. and R.J.B.; methodology, S.C.P. and R.J.B.; software, S.C.P.; validation, S.C.P. and R.J.B.; formal analysis, S.C.P.; investigation, S.C.P., J.J.C., and R.J.B.; resources, S.C.P.; data curation, S.C.P. and J.J.C.; writing—original draft preparation, S.C.P. and R.J.B.; writing—review and editing, S.C.P., J.J.C., and R.J.B.; visualization, S.C.P.; supervision, S.C.P.; project administration, S.C.P. and R.J.B.; funding acquisition, S.C.P. and R.J.B. All authors have read and agreed to the published version of the manuscript.

Funding: This research was funded by the U.S. National Science Foundation (2329911), Sandia National Laboratory (DE-NA0003525), and U.S. Department of Energy (DE-SC0016605). Computational resources used in these analyses are provided by the NSF Extreme Science and Engineering Discovery Environment (XSEDE2) (award TG-ATM170024).

Data Availability Statement: Data from the National Weather Service Automated Surface Observing System network are available for download from: <https://www.ncei.noaa.gov/products/land-based-station/automated-surface-weather-observing-systems> (last accessed 14 November 2024). Data from the NASA Passive Microwave Hail Climatology Data Products V1 dataset shown in Figure 2 are available for download from: <https://search.earthdata.nasa.gov/> (last accessed 21 July 2022). The LEE atlas for CONUS can be downloaded from ZENODO, doi: 10.5281/zenodo.14247620.

Acknowledgments: The authors gratefully acknowledge the scientists and engineers responsible for the ASOS network and the comments of two anonymous reviewers.

Conflicts of Interest: The authors declare no conflicts of interest.

References

1. Barthelmie, R.J.; Pryor, S.C. Potential contribution of wind energy to climate change mitigation. *Nat. Clim. Change* **2014**, *4*, 684–688. [CrossRef]
2. Barthelmie, R.J.; Pryor, S.C. Climate Change Mitigation Potential of Wind Energy. *Climate* **2021**, *9*, 136. [CrossRef]
3. GWEC. *Global Wind Report 2024*; Global Wind Energy Council: Brussels, Belgium, 2024; p. 168. Available online: <https://gwec.net/global-wind-report-2024/> (accessed on 5 September 2024).
4. Lazard. Lazard's Levelized Cost of Energy Analysis—Version 16.0; Zurich, Switzerland; 2023. Available online: <https://www.lazard.com/research-insights/levelized-cost-of-energyplus/> (accessed on 5 September 2024).
5. Xu, J.; Zou, J.; Ziegler, A.D.; Wu, J.; Zeng, Z. What drives the change of capacity factor of wind turbine in the United States? *Environ. Res. Lett.* **2023**, *18*, 064009. [CrossRef]
6. Wisler, R.; Rand, J.; Seel, J.; Beiter, P.; Baker, E.; Lantz, E.; Gilman, P. Expert elicitation survey predicts 37% to 49% declines in wind energy costs by 2050. *Nat. Energy* **2021**, *6*, 555–565. [CrossRef]
7. Enevoldsen, P.; Xydis, G. Examining the trends of 35 years growth of key wind turbine components. *Energy Sustain. Dev.* **2019**, *50*, 18–26. [CrossRef]
8. Bolinger, M.; Wisler, R.; O'Shaughnessy, E. Levelized cost-based learning analysis of utility-scale wind and solar in the United States. *iScience* **2022**, *25*, 104378. [CrossRef] [PubMed]
9. Wisler, R.H.; Bolinger, M.; Lantz, E. Assessing wind power operating costs in the United States: Results from a survey of wind industry experts. *Renew. Energy Focus* **2019**, *30*, 46–57. [CrossRef]
10. Brøndsted, P.; Nijssen, R.P.; Goutianos, S. *Advances in Wind Turbine Blade Design and Materials*; Woodhead Publishing: Cambridge, UK, 2023.
11. Du, Y.; Zhou, S.; Jing, X.; Peng, Y.; Wu, H.; Kwok, N. Damage detection techniques for wind turbine blades: A review. *Mech. Syst. Signal Process.* **2020**, *141*, 106445. [CrossRef]
12. Liu, D.; da Fonseca, L.G. *Global Onshore Wind Power Operations & Maintenance (O&M) 2020*; Wood Mackenzie: Edinburgh, UK, 2021. Available online: <https://www.woodmac.com/reports/power-markets-global-onshore-wind-power-operations-and-maintenance-oandm-2020-467883/> (accessed on 5 September 2024).
13. Mishnaevsky, L., Jr.; Thomsen, K. Costs of repair of wind turbine blades: Influence of technology aspects. *Wind. Energy* **2020**, *23*, 2247–2255. [CrossRef]
14. Mishnaevsky Jr, L.; Frost-Jensen Johansen, N.; Fraisse, A.; Fæster, S.; Jensen, T.; Bendixen, B. Technologies of wind turbine blade repair: Practical comparison. *Energies* **2022**, *15*, 1767. [CrossRef]
15. Sun, S.; Wang, T.; Yang, H.; Chu, F. Damage identification of wind turbine blades using an adaptive method for compressive beamforming based on the generalized minimax-concave penalty function. *Renew. Energy* **2022**, *181*, 59–70. [CrossRef]
16. Santelo, T.N.; de Oliveira, C.M.R.; Maciel, C.D.; de Monteiro, A.J.R.B. Wind turbine failures review and trends. *J. Control Autom. Electr. Syst.* **2022**, *33*, 505–521. [CrossRef]
17. Ozturk, S.; Fthenakis, V. Predicting frequency, time-to-repair and costs of wind turbine failures. *Energies* **2020**, *13*, 1149. [CrossRef]
18. Pryor, S.C.; Barthelmie, R.J.; Coburn, J.J.; Zhou, X.; Rodgers, M.; Norton, H.; Campobasso, M.S.; López, B.M.; Hasager, C.B.; Mishnaevsky Jr, L. Prioritizing Research for Enhancing the Technology Readiness Level of Wind Turbine Blade Leading-Edge Erosion Solutions. *Energies* **2024**, *17*, 6285. [CrossRef]
19. Maniaki, D.C.; MacDonald, H.; Paquette, J.; Clarke, R. *Leading Edge Erosion Classification System*; Technical Report from IEA Wind Task 46 Erosion of Wind Turbine Blades; Sandia National Lab: Albuquerque, NM, USA, 2022; 52p. Available online: <https://iea-wind.org/task46/t46-results/> (accessed on 5 September 2024).
20. Mishnaevsky Jr, L.; Hasager, C.B.; Bak, C.; Tilg, A.-M.; Bech, J.I.; Rad, S.D.; Fæster, S. Leading edge erosion of wind turbine blades: Understanding, prevention and protection. *Renew. Energy* **2021**, *169*, 953–969. [CrossRef]
21. Sareen, A.; Sapre, C.A.; Selig, M.S. Effects of leading edge erosion on wind turbine blade performance. *Wind Energy* **2014**, *17*, 1531–1542. [CrossRef]

22. Gaudern, N. A practical study of the aerodynamic impact of wind turbine blade leading edge erosion. *J. Phys. Conf. Ser.* **2014**, *524*, 012031. [CrossRef]
23. Froese, M. Wind-farm owners can now detect leading-edge erosion from data alone. *Windpower Engineering and Development*, 14 August 2018. Available online: <https://www.windpowerengineering.com/wind-farm-owners-can-now-detect-leading-edge-erosion-from-data-alone/> (accessed on 5 September 2024).
24. Campobasso, M.S.; Castorrini, A.; Ortolani, A.; Minisci, E. Probabilistic analysis of wind turbine performance degradation due to blade erosion accounting for uncertainty of damage geometry. *Renew. Sustain. Energy Rev.* **2023**, *178*, 113254. [CrossRef]
25. Xiaoxun, Z.; Xinyu, H.; Xiaoxia, G.; Xing, Y.; Zixu, X.; Yu, W.; Huaxin, L. Research on crack detection method of wind turbine blade based on a deep learning method. *Appl. Energy* **2022**, *328*, 120241. [CrossRef]
26. Kong, K.; Dyer, K.; Payne, C.; Hamerton, I.; Weaver, P.M. Progress and trends in damage detection methods, maintenance, and data-driven monitoring of wind turbine blades—A review. *Renew. Energy Focus* **2023**, *44*, 390–412. [CrossRef]
27. DNV. *DNV-RP-0573 Evaluation of Erosion and Delamination for Leading Edge Protection Systems of Rotor Blades*; Det Norske Veritas: Høvik, Norway, 2021; 44p.
28. Lopez, J.C.; Kolios, A.; Wang, L.; Chiachio, M.; Dimitrov, N. Reliability-based leading edge erosion maintenance strategy selection framework. *Appl. Energy* **2024**, *358*, 122612. [CrossRef]
29. Law, H.; Koutsos, V. Leading edge erosion of wind turbines: Effect of solid airborne particles and rain on operational wind farms. *Wind Energy* **2020**, *23*, 1955–1965. [CrossRef]
30. Boopathi, K.; Mishnaevsky Jr, L.; Sumantraa, B.; Premkumar, S.A.; Thamodharan, K.; Balaraman, K. Failure mechanisms of wind turbine blades in India: Climatic, regional, and seasonal variability. *Wind Energy* **2022**, *25*, 968–979. [CrossRef]
31. Walzberg, J.; Cooperman, A.; Watts, L.; Eberle, A.L.; Carpenter, A.; Heath, G.A. Regional representation of wind stakeholders' end-of-life behaviors and their impact on wind blade circularity. *iScience* **2022**, *25*, 104734. [CrossRef] [PubMed]
32. Bech, J.I.; Hasager, C.B.; Bak, C. Extending the life of wind turbine blade leading edges by reducing the tip speed during extreme precipitation events. *Wind Energy Sci.* **2018**, *3*, 729–748. [CrossRef]
33. Bartolomé, L.; Teuwen, J. Prospective challenges in the experimentation of the rain erosion on the leading edge of wind turbine blades. *Wind Energy* **2019**, *22*, 140–151. [CrossRef]
34. Zhang, S.; Dam-Johansen, K.; Nørkjær, S.; Bernad, P.L., Jr.; Kiil, S. Erosion of wind turbine blade coatings—design and analysis of jet-based laboratory equipment for performance evaluation. *Prog. Org. Coat.* **2015**, *78*, 103–115. [CrossRef]
35. Pryor, S.C.; Barthelmie, R.J.; Cadence, J.; Dellwik, E.; Hasager, C.B.; Kral, S.T.; Reuder, J.; Rodgers, M.; Veraart, M. Atmospheric Drivers of Wind Turbine Blade Leading Edge Erosion: Review and Recommendations for Future Research. *Energies* **2022**, *15*, 8553. [CrossRef]
36. Letson, F.; Barthelmie, R.J.; Pryor, S.C. RADAR-derived precipitation climatology for wind turbine blade leading edge erosion. *Wind Energy Sci.* **2020**, *5*, 331–347. [CrossRef]
37. Doagou-Rad, S.; Mishnaevsky Jr, L. Rain erosion of wind turbine blades: Computational analysis of parameters controlling the surface degradation. *Meccanica* **2020**, *55*, 725–743. [CrossRef]
38. Verma, A.S.; Castro, S.G.; Jiang, Z.; Teuwen, J.J. Numerical investigation of rain droplet impact on offshore wind turbine blades under different rainfall conditions: A parametric study. *Compos. Struct.* **2020**, *241*, 112096. [CrossRef]
39. Tempelis, A.; Jespersen, K.M.; Mishnaevsky, L., Jr. Fatigue damage mechanics approach to predict the end of incubation and breakthrough of leading edge protection coatings for wind turbine blades. *Int. J. Fatigue* **2025**, *190*, 108617. [CrossRef]
40. Rinker, J.; Dykes, K.L. *WindPACT Reference Wind Turbines*; NREL/TP-5000-67667; National Renewable Energy Lab. (NREL): Golden, CO, USA, 2018. Available online: <https://www.nrel.gov/docs/fy18osti/67667.pdf> (accessed on 5 September 2024).
41. Gunn, R.; Kinzer, G.D. The terminal velocity of fall for water droplets in stagnant air. *J. Atmos. Sci.* **1949**, *6*, 243–248. [CrossRef]
42. Marshall, J.S.; Palmer, W.M.K. The distribution of raindrops with size. *J. Meteorol.* **1948**, *5*, 165–166. [CrossRef]
43. Best, A. The size distribution of raindrops. *Q. J. R. Meteorol. Soc.* **1950**, *76*, 16–36. [CrossRef]
44. Springer, G.S.; Baxi, C.B. A model for rain erosion of homogeneous materials. In *Erosion, Wear, and Interfaces with Corrosion*; ASTM International: West Conshohocken, PA, USA, 1974; pp. 106–124.
45. Springer, G.S.; Yang, C.-I.; Larsen, P.S. Analysis of rain erosion of coated materials. *J. Compos. Mater.* **1974**, *8*, 229–252. [CrossRef]
46. Letson, F.; Pryor, S.C. From Hydrometeor Size Distribution Measurements to Projections of Wind Turbine Blade Leading Edge Erosion. *Energies* **2023**, *5*, 3906. [CrossRef]
47. Johnston, B.; Foley, A.; Doran, J.; Littler, T. Levelised cost of energy, A challenge for offshore wind. *Renew. Energy* **2020**, *160*, 876–885. [CrossRef]
48. Đukan, M.; Gumber, A.; Egli, F.; Steffen, B. The role of policies in reducing the cost of capital for offshore wind. *iScience* **2023**, *26*, 106945. [CrossRef] [PubMed]
49. Hoen, B.D.; Diffendorfer, J.E.; Rand, J.T.; Kramer, L.A.; Garrity, C.P.; Hunt, H.E. *United States Wind Turbine Database (v6.1, November 2023)*; U.S. Geological Survey, American Clean Power Association, and Lawrence Berkeley National Laboratory Data Release; United States Geological Survey: Reston, VA, USA, 2018.

50. Rand, J.T.; Kramer, L.A.; Garrity, C.P.; Hoen, B.D.; Diffendorfer, J.E.; Hunt, H.E.; Spears, M. A continuously updated, geospatially rectified database of utility-scale wind turbines in the United States. *Sci. Data* **2020**, *7*, 15. [CrossRef]
51. Bang, S.D.; Cecil, D.J. Constructing a multifrequency passive microwave hail retrieval and climatology in the GPM domain. *J. Appl. Meteorol. Climatol.* **2019**, *58*, 1889–1904. [CrossRef]
52. Mishnaevsky Jr, L.; Tempelis, A.; Kuthe, N.; Mahajan, P. Recent developments in the protection of wind turbine blades against leading edge erosion: Materials solutions and predictive modelling. *Renew. Energy* **2023**, *215*, 118966. [CrossRef]
53. Frost-Jensen Johansen, N.; Mishnaevsky Jr, L.; Dashtkar, A.; Williams, N.A.; Fæster, S.; Silvello, A.; Cano, I.G.; Hadavinia, H. Nanoengineered graphene-reinforced coating for leading edge protection of wind turbine blades. *Coatings* **2021**, *11*, 1104. [CrossRef]
54. Fæster, S.; Johansen, N.F.J.; Mishnaevsky Jr, L.; Kusano, Y.; Bech, J.I.; Madsen, M.B. Rain erosion of wind turbine blades and the effect of air bubbles in the coatings. *Wind Energy* **2021**, *24*, 1071–1082. [CrossRef]
55. Herring, R.; Dyer, K.; Martin, F.; Ward, C. The increasing importance of leading edge erosion and a review of existing protection solutions. *Renew. Sustain. Energy Rev.* **2019**, *115*, 109382. [CrossRef]
56. Ansari, Q.M.; Sánchez, F.; Mishnaevsky, L., Jr.; Young, T.M. Evaluation of offshore wind turbine blades coating thickness effect on leading edge protection system subject to rain erosion. *Renew. Energy* **2024**, *226*, 120378. [CrossRef]
57. Major, D.; Palacios, J.; Maughmer, M.; Schmitz, S. Aerodynamics of leading-edge protection tapes for wind turbine blades. *Wind Eng.* **2021**, *45*, 1296–1316. [CrossRef]
58. Katsivalis, I.; Chanteli, A.; Finnegan, W.; Young, T.M. Mechanical and interfacial characterisation of leading-edge protection materials for wind turbine blade applications. *Wind Energy* **2022**, *25*, 1758–1774. [CrossRef]
59. Coburn, J.J.; Pryor, S.C. Projecting future energy production from operating wind farms in North America: Part 3: Variability. *J. Appl. Meteorol. Climatol.* **2023**, *62*, 1523–1537. [CrossRef]
60. Jeon, H.; Hartman, B.; Cutler, H.; Hill, R.; Hu, Y.; Lu, T.; Shields, M.; Turner, D.D. Estimating the economic impacts of improved wind speed forecasts in the United States electricity sector. *J. Renew. Sustain. Energy* **2022**, *14*, 036101. [CrossRef]
61. Huff, F. Time distribution characteristics of rainfall rates. *Water Resour. Res.* **1970**, *6*, 447–454. [CrossRef]
62. Huff, F.A.; Neill, J.C. Frequency of point and areal mean rainfall rates. *Eos Trans. Am. Geophys. Union* **1956**, *37*, 679–681.
63. Kursinski, A.L.; Zeng, X. Areal estimation of intensity and frequency of summertime precipitation over a midlatitude region. *Geophys. Res. Lett.* **2006**, *33*, L22401. [CrossRef]
64. Cook, N.J. Locating the anemometers of the US ASOS network and classifying their local shelter. *Weather* **2022**, *77*, 256–263. [CrossRef]
65. McNitt, J.A.; Facundo, J. An overview of the Federal Government’s Automated Surface Observing System sustainment activity. In Proceedings of the 13th American Meteorological Society Conference on Integrated Observing and Assimilation Systems for Atmosphere, Oceans, and Land Surface, Pheonix, AZ, USA, 11–15 January 2009.
66. Cook, N.J. Curating the TD6405 database of 1-min interval wind observations across the USA for use in Wind Engineering studies. *J. Wind. Eng. Ind. Aerodyn.* **2022**, *224*, 104961. [CrossRef]
67. Schmitt, I.V.; Chester, V. A quality control algorithm for the ASOS ice free wind sensor. In Proceedings of the 13th American Meteorological Society Conference on Integrated Observing and Assimilation Systems for Atmosphere, Oceans, and Land Surface, Pheonix, AZ, USA, 11–15 January 2009.
68. National Oceanic Atmospheric Administration. *Automated Surface Observing System (ASOS) User’s Guide*; National Oceanic Atmospheric Administration: Silver Spring, MD, USA, 1998.
69. Butler, R.D.; McKee, T.B. *ASOS Heated Tipping Bucket Performance Assessment and Impact on Precipitation Climate Continuity*; Libraries: NASA 19990025176; Colorado State University: Fort Collins, CO, USA, 1998; Available online: <https://apps.dtic.mil/sti/citations/ADA359136> (accessed on 5 September 2024).
70. White, S.G.; Winans, L.J.; Fiore Jr, J.V. Development of the all-weather precipitation accumulation gauge for ASOS. In Proceedings of the American Meteorological Society Eighth Symposium on Integrated Observing and Assimilation Systems for Atmosphere, Oceans, and Land Surface, Seattle, WA, USA, 11–15 January 2004.
71. Irwin, J.S. A theoretical variation of the wind profile power-law exponent as a function of surface roughness and stability. *Atmos. Environ.* **1979**, *13*, 191–194. [CrossRef]
72. Letson, F.; Shepherd, T.J.; Barthelmie, R.J.; Pryor, S.C. WRF modelling of deep convection and hail for wind power applications. *J. Appl. Meteorol. Climatol.* **2020**, *59*, 1717–1733. [CrossRef]
73. Pryor, S.; Letson, F.; Shepherd, T.; Barthelmie, R. Evaluation of WRF simulation of deep convection in the US Southern Great Plains. *J. Appl. Meteorol. Climatol.* **2023**, *62*, 41–62. [CrossRef]
74. Pryor, S.C.; Barthelmie, R.J. Wind shadows impact planning of large offshore wind farms. *Appl. Energy* **2024**, *359*, 122755. [CrossRef]
75. Eisenberg, D.; Laustsen, S.; Stege, J. Wind turbine blade coating leading edge rain erosion model: Development and validation. *Wind Energy* **2018**, *21*, 942–951. [CrossRef]
76. Castorrini, A.; Venturini, P.; Bonfiglioli, A. Generation of Surface Maps of Erosion Resistance for Wind Turbine Blades under Rain Flows. *Energies* **2022**, *15*, 5593. [CrossRef]
77. Springer, G.S. *Erosion by Liquid Impact*; John Wiley and Sons: New York, NY, USA, 1976; p. 278.

78. Herring, R.; Domenech, L.; Renau, J.; Šakalytė, A.; Ward, C.; Dyer, K.; Sánchez, F. Assessment of a wind turbine blade erosion lifetime prediction model with industrial protection materials and testing methods. *Coatings* **2021**, *11*, 767. [CrossRef]
79. Hoksbergen, N.; Akkerman, R.; Baran, I. The Springer model for lifetime prediction of wind turbine blade leading edge protection systems: A review and sensitivity study. *Materials* **2022**, *15*, 1170. [CrossRef] [PubMed]
80. Villarini, G.; Smith, J.A.; Baeck, M.L.; Marchok, T.; Vecchi, G.A. Characterization of rainfall distribution and flooding associated with US landfalling tropical cyclones: Analyses of Hurricanes Frances, Ivan, and Jeanne (2004). *J. Geophys. Res. Atmos.* **2011**, *116*, D23116. [CrossRef]
81. Brauer, N.S.; Basara, J.B.; Homeyer, C.R.; McFarquhar, G.M.; Kirstetter, P.E. Quantifying precipitation efficiency and drivers of excessive precipitation in post-landfall Hurricane Harvey. *J. Hydrometeorol.* **2020**, *21*, 433–452. [CrossRef]
82. Mass, C. *The Weather of the Pacific Northwest*; University of Washington Press: Lanham, MD, USA, 2021; 312p, ISBN 9780295748443.
83. Papadakis, M.; Wong, S.-C.; Rachman, A.; Hung, K.E.; Vu, G.T.; Bidwell, C.S. *Large and Small Droplet Impingement Data on Airfoils and Two Simulated Ice Shapes*; NASA, Report #E-15275; Glenn Research Center: Cleveland, OH, USA, 2007. Available online: <https://ntrs.nasa.gov/citations/20070034950> (accessed on 5 September 2024).
84. Heymsfield, A.; Szakáll, M.; Jost, A.; Giammanco, I.; Wright, R. A comprehensive observational study of graupel and hail terminal velocity, mass flux, and kinetic energy. *J. Atmos. Sci.* **2018**, *75*, 3861–3885. [CrossRef]
85. Keegan, M.H.; Nash, D.; Stack, M. On erosion issues associated with the leading edge of wind turbine blades. *J. Phys. D Appl. Phys.* **2013**, *46*, 383001. [CrossRef]
86. Kim, H.; Kedward, K.T. Modeling hail ice impacts and predicting impact damage initiation in composite structures. *AIAA J.* **2000**, *38*, 1278–1288. [CrossRef]
87. Macdonald, J.; Stack, M. Some thoughts on modelling hail impact on surfaces. *J. Bio-Tribo-Corros.* **2021**, *7*, 1–7. [CrossRef]
88. Zhu, X.; Fu, X.; Liu, L.; Xu, K.; Luo, G.; Zhao, Z.; Chen, W. Damage mechanism of composite laminates under multiple ice impacts at high velocity. *Int. J. Impact Eng.* **2022**, *168*, 104296. [CrossRef]
89. Wisner, R.H.; Bolinger, M. *Benchmarking Anticipated Wind Project Lifetimes: Results from a Survey of US Wind Industry Professionals*; Berkeley Lab, Electricity Markets and Policy Group: San Francisco, CA, USA, 2019. Available online: <https://emp.lbl.gov/publications/benchmarking-anticipated-wind-project> (accessed on 5 September 2024).
90. Hasager, C.; Vejen, F.; Bech, J.; Skrzypiąski, W.; Tilg, A.-M.; Nielsen, M. Assessment of the rain and wind climate with focus on wind turbine blade leading edge erosion rate and expected lifetime in Danish Seas. *Renew. Energy* **2020**, *149*, 91–102. [CrossRef]
91. Hannesdóttir, Á.; Kral, S.T.; Reuder, J.; Hasager, C.B. Rain erosion atlas for wind turbine blades based on ERA5 and NORA3 for Scandinavia. *Results Eng.* **2024**, *22*, 102010. [CrossRef]
92. Bartolomé, L.; Teuwen, J. Methodology for the energetic characterisation of rain erosion on wind turbine blades using meteorological data: A case study for The Netherlands. *Wind Energy* **2021**, *24*, 686–698. [CrossRef]

Disclaimer/Publisher’s Note: The statements, opinions and data contained in all publications are solely those of the individual author(s) and contributor(s) and not of MDPI and/or the editor(s). MDPI and/or the editor(s) disclaim responsibility for any injury to people or property resulting from any ideas, methods, instructions or products referred to in the content.